Journal of Interfaces, Thin films, and Low dimensional systems 4 (1) Summer and Autumn (2020) 357-364

Deposition of TiCrN on silicon substrate using radio frequency magnetron sputtering

Scientific research paper

Samira Nassiri and Eslam Ghareshabani*

Faculty of Physics, Sahand University of Technology, Tabriz, Iran

ARTICLE INFO

Article history:
Received 30 March 2021
Revised 26 August 2021
Accepted 27 August 2021
Available online 30 October 2021

Keywords:
Titanium chromium nitride,
RF magnetron sputtering
Bias voltage
GIXRD
FE-SEM

ABSTRACT

The ternary titanium chromium nitride (TiCrN) thin film on Si (100) substrate without any external temperature was deposited by radio frequency (RF) magnetron sputtering. The substrate was kept at a distance of 35 mm from the target. The growth morphology, crystalline structure, roughness, contact angle, and thickness of the coatings were studied as a function of the input RF power and negative bias voltage. The grazing incident X-ray diffraction (GIXRD) results show that TiCrN diffraction peaks appeared only in samples with substrate bias = -70 V. The surface morphology was investigated by Atomic force microscopy (AFM) and field emission scanning electron microscopy (FESEM). The films change from hydrophilic to hydrophobic with the increase of negative bias voltage. The roughness and contact angle of the samples increase with the decrease in the RF power from 300 W to 200 W. In both cases (a) and (b), the deposition rate increases as a result of increase in the target power.

1 Introduction

Of the physical methods to construct ternary metal nitrides coatings on an appropriate substrate is the physical vapor deposition (PVD) method, that magnetron sputtering method is one of the PVD methods that include direct current (DC) sputtering and radio frequency (RF) sputtering [1, 2]. The physical vapor deposition technique for deposition of hard coatings has developed because of their wide range of applications in industry and research such as machine parts and cutting tools [3]. The thickness of the coating can also be entirely controlled by this method [4].

The binary nitrides coatings such as TiN, CrN, and ZrN are commonly utilized to improve the chemical and mechanical properties like high hardness, low friction coefficient, and good corrosion resistance of materials. Despite their perfect properties, the coatings show insufficient properties for some applications. For example, TiN and CrN coatings are degraded by oxidation during machining process at high temperatures above 600° C and 800° C, respectively [5]. Therefore, in order to suppress this problem, by incorporation additional metals such as Al, Zr, Cr, and V, coatings consisting of ternary mixed phases with improved properties can be obtained. However, the stability of the physical-mechanical features of such coatings under irradiation is inadequately studied which prevents their possible use as radiation-resistant protective coatings [6]. By Comparing with binary nitride hard coatings, the ternary coatings are very flexible due to their performances which may be tailored for various applications [7, 8]. Furthermore, the nanocrystalline structure more easily is created in ternary multi-coatings than binary coatings, because of addition atoms impede the base-phase growing in the

*Corresponding author.
Email address: e.ghareshabani@Gmail.com
DOI: 10.22051/jitl.2021.35578.1052

deposition. Most of the transition ternary metal nitrides such as TiAlN, TiCrN, and AlCrN are multi-phase materials by different PVD techniques [7]. Among these films, the TiCrN thin film because of its excellent features such as high hardness, high temperature oxidation resistance, low friction coefficient, and high chemical wear resistance [9-11] has attracted more attention.

In general, ternary nitride films such as TiAlN [12-15], TiZrN [16, 17], TiVN [9], TiCrN [10] and CrAlN [18-27] were investigated by different techniques. For example, by reactive DC magnetron co-sputtering on a silicon substrate [3], ion beam assisted deposition [28], medium frequency magnetron sputtering [29], cathodic arc deposition [30], arc ion plating [31], and closed – field unbalanced magnetron sputtering [32, 33]. In this study, we deposited the TiCrN thin films on Si (100) substrates by the radio frequency (RF) magnetron sputtering method without any external temperature. We reported effects of the RF power and bias voltage on structural properties, thickness, and surface roughness of thin films.

2 Experimental setup

In this study, the TiCrN thin films on the Si (100) substrate were deposited using RF magnetron sputtering at room temperature. This device (Fig. 1) includes a cylindrical stainless steel chamber, two pumps, a pressure gauge device to control inside of the deposition chamber pressure, and a power supply connected to the deposition chamber. Inside the deposition chamber, there is a Ti-Cr target with 2 inches diameter and a substrate holder that was mounted in the upper part of the chamber.

During the coating process, high purity Ar (99.999 wt %) and N_2 (99.999 wt %) were used as process gases while their flow rates were regulated by mass flow controllers. Since the substrate that we used, the Si (100) has an oxide layer (SiO_2) at its surface, we washed it in hydrofluoric acid (HF) to remove the oxide layer for about one minute. Then, washed the substrate in the ultrasonic bath acetone, ethanol, and distilled water respectively for approximately 10 minutes to remove contaminations and impurities. After cleaning the substrate, it was thoroughly dried and installed at the sample holder. The vacuum chamber was evacuated to base pressure of 10^{-5} mbar using a diffusion pump. Before deposition process, Ar gas was introduced into the vacuum chamber to pre-sputter for 15 min to remove any impurity on the Ti-Cr target. The deposition pressure and the distance between target and substrate were kept at 0.02 mbar and35 mm, respectively. The detailed deposition parameters for the TiCrN thin films on the Si (100) substrate were presented in Table 1. All the deposition processes were carried out at an ambient temperature. All the samples were deposited for 1 h.

Table 1. The deposition parameters for the TiCrN thin films on the Si (100) substrate.

	Sample Number	Base pressure (mbar)	Power (W)	Bias voltage (V)	Ar/N_2 Ratio	Deposition time (min)	Working pressure (mbar)
(a)	1	10^{-5}	300	-	1	100	0.02
	2	10^{-5}	250	-	1	100	0.02
(b)	3	10^{-5}	300	-70	1	100	0.02
	4	10^{-5}	250	-70	1	100	0.02

In this article, we report the synthesis of TiCrN thin films using the radio frequency (RF) magnetron sputtering method. The structural properties of the deposited thin films were evaluated using grazing incidence X-ray diffractometer (GIXRD; Philips X'pert PW1730, Netherlands) analysis equipped with a Cu Kα X-radiation (40 kV, 40 mA, 0.15406 nm), step size of 0.05°, and count time of one second per step. Field emission scanning electron microscopy (FESEM; FEI ESEM QUANTA 200) equipped with an EDX analysis working at an acceleration voltage of 12 kV was provided to analyze the morphological properties and the chemical composition of the samples.

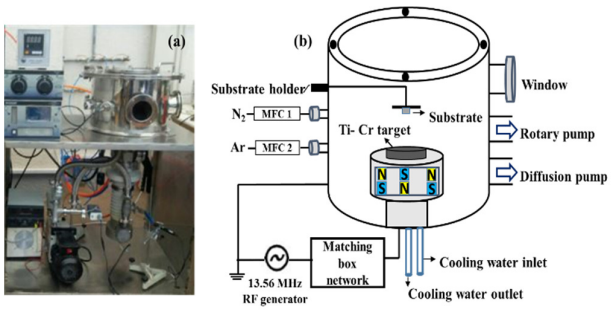

Figure 1. (a) RF magnetron sputtering device and (b) A scheme from inside this device.

The roughness of the samples was obtained using an atomic force microscope (AFM; Bruker, Billerica, USA) with a scan size of 5×5 μm^2 and a scan rate of 1

Hz. The wettability of the surface of the coatings was also evaluated by measuring the contact angle of deionized water on the specimens using a contact angle measurement instrument.

3 Results and discussion

3.1 GIXRD analysis

Figure 2 shows the results of GIXRD patterns of the TiCrN thin films deposited on Si (100) substrates for the input power of 250 W (samples 2 and 4). In these patterns, four compounds, including TiCrN, TiN, Ti_2N, and CrN are seen. In sample 2, the pattern exhibits the diffraction peaks associated with CrN, Ti_2N, and Si. The diffraction peaks 2Θ =25° (Powder Diffraction Patterns: 96-110-0032), 37.50, 43.6^0 and 63.4^0 (Powder Diffraction Patterns: 96-100-8957) are related to Ti_2N (110), CrN (111), CrN (200) and CrN (220), respectively. The diffraction peaks 2Θ = 33^0 and 45.1^0 are related to Si (211) and Si (400), respectively. In sample 4, the pattern exhibits the diffraction peaks related to TiCrN, TiN, CrN, and Si. Considering the TiN (200) at diffraction angle 2Θ = 42.5^0, CrN and Ti_2N peaks, it is observed that the TiCrN (200) and TiCrN (220) peaks are in the range of these compounds [3,30,32].

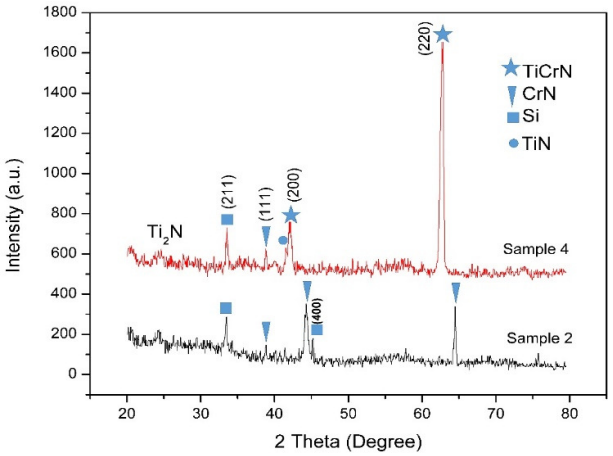

Figure 2. GIXRD patterns of samples 2 and 4 (input power of 250 W).

Figure 3 shows the results of GIXRD patterns of the TiCrN thin films deposited on Si (100) substrates for the input power of 300 W (samples 1 and 3). In sample 1, CrN (111), TiN (200) and TiN (220) compounds and Si (211), and in sample 3, CrN (111), TiCrN (200), Ti_2N (110), Si (002) and TiCrN (220) compounds are seen. When the bias voltage increases from 0 V to -70 V, two phases related to TiCrN are observed. The emergence of these new induced phases can be due to the fact that the energy and flux of the ions are increased. As a result, a large number of target ion species arrived on the growing film that lead to the stoichiometry changes at the film to form a new phase TiCrN. Also, thin film thickness and the intensity of TiCrN (220) diffraction peak decrease as the RF power increases from 250 W in sample 4 to 300 W in sample 3. This can be attributed to the etching effect.

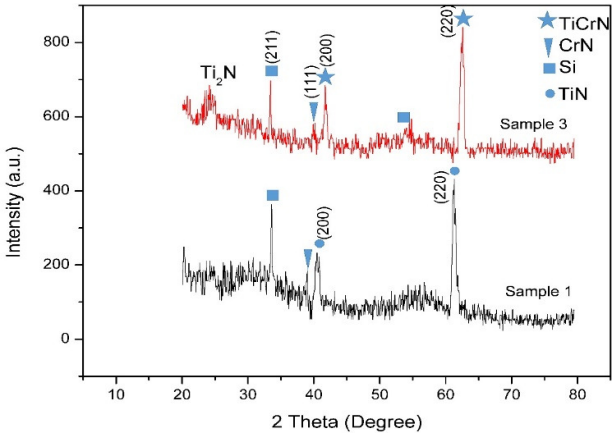

Figure 3. GIXRD patterns of samples 1 and 3 (input power of 300 W).

3.2 FESEM and EDS Analysis

In this study, the ternary nitride nanostructured TiCrN thin films were deposited successfully on Si (100) substrates at two cases: (a) without any bias voltage; (b) with a bias voltage = -70 V with the same deposition parameters. The field emission scanning electron microscopy micrographs are shown in Fig. 4. The morphology of all samples shows an entirely homogeneous and uniform surface of the TiCrN thin films. By comparing the samples without bias and samples with bias voltage, we observe that for the samples with bias voltage, the grain size becomes larger while the shape of the particles change. By comparing the input power, we see that as the input power increases in both cases (a) and (b), the grain size becomes smaller and the particle agglomeration increases.

From the cross-sectional FE-SEM images, as shown in Fig. 5, it turns out that the thickness of the coating in samples without bias voltage is greater than

the bias voltage samples. We observe that as the input power increases in both cases (a) and (b), the coating

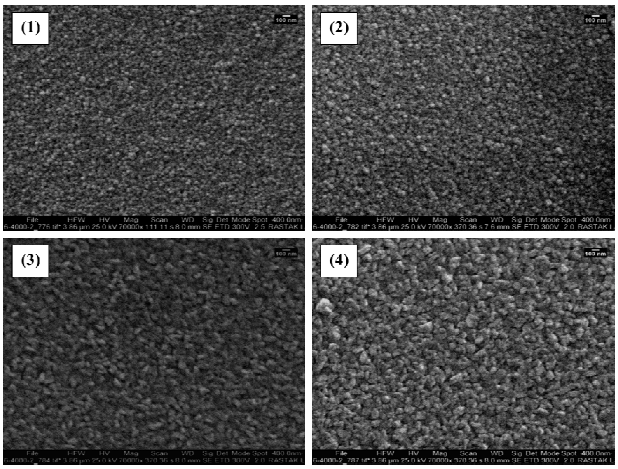

Figure 4. FE-SEM micrographs of the TiCrN thin films.

thickness increases. With increasing the input power from 250 W to 300W, the coating thickness increases from 662 nm to 782 nm in case of without any bias voltage, and from 599 nm to 719 nm in case of with bias voltage. Also, by comparing (a) and (b) samples, we observed a decrease in coating thickness in the samples with a bias voltage.

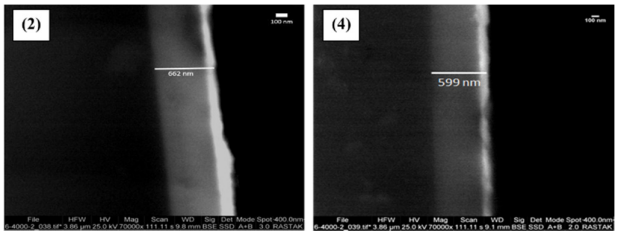

Figure 5: Cross-sectional FE-SEM morphology of the TiCrN thin films for samples 2 and 4.

According to results of the EDS analysis, it is observed that under the same conditions, in the sample without the bias voltage, more atoms of titanium, chromium, and nitrogen are deposited on the substrate. By comparing the input power, we observe that with increasing the input power in both cases, the number of atoms deposited on the substrate increases. Figure 6 shows a typical EDS spectrum and atomic percentages of Ti, Cr, N, and Si for sample 2.

In Fig. 7, the distribution of each of the atoms is shown, which is taken by mapping analysis. Images represent the successful deposition of all atoms on the substrate. Also, line scan analysis results show the successful deposition of TiCrN thin films on the Si (100) process. This analysis exhibit that with approaches to the sample surface, the presence of Ti, Cr, and N atoms increase. The images for this analysis is shown in Fig. 8.

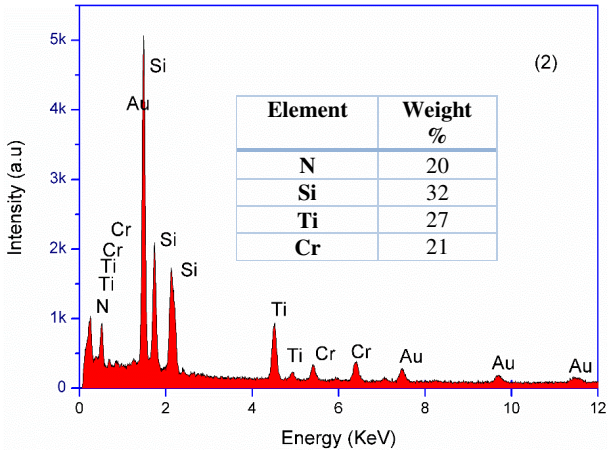

Figure 6: Typical EDS spectrum of the sample 2.

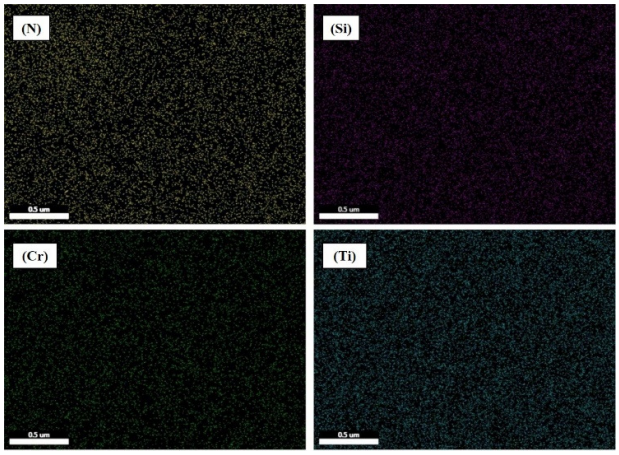

Figure 7: Typical elemental mapping analysis of nitrogen, silicon, chromium, and titanium on the surface of sample 2.

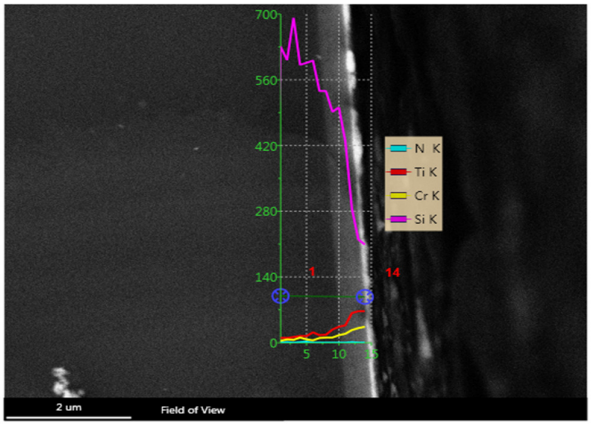

Figure 8. Line scan analysis image of TiCrN thin films related to sample 2.

3.3 AFM results

Atomic force microscopy (AFM) images of TiCrN thin films are shown in Fig. 9 (Fig. 9A: 2D and Fig. 9B: 3D images). In this study, the AFM in contact mode is used to scan the area of 5 µm ×5 µm.

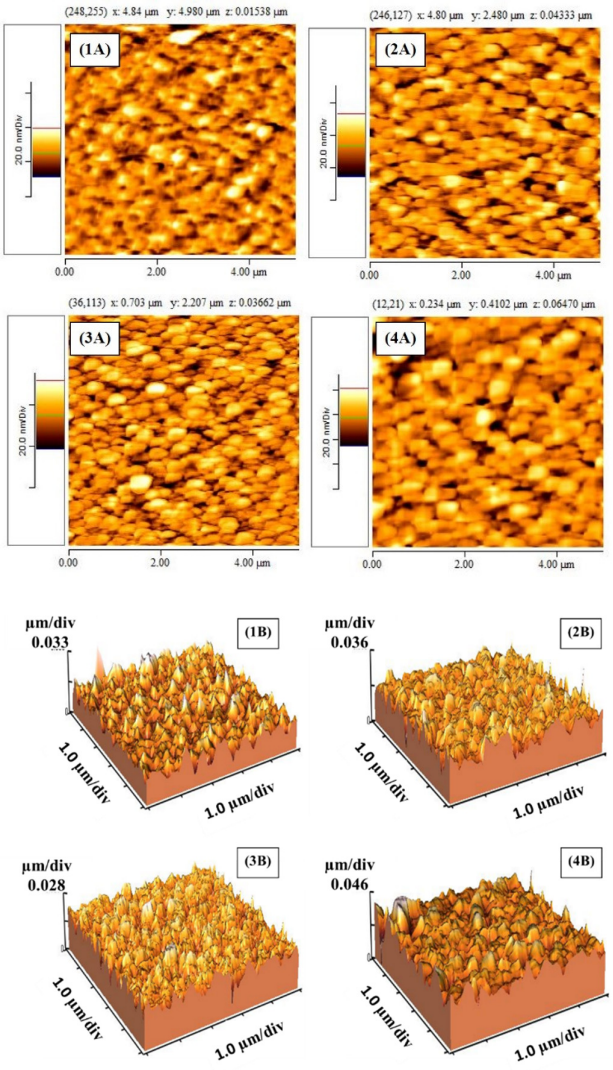

Figure 9. (A) 2D-AFM images of the samples deposited and (B) 3D-AFM images of the samples deposited.

With increasing the input power, we observe that the root mean square (RMS) roughness and average roughness (Ra) values of TiCrN thin films decreases. in case (a), by increasing the input power from 250 W to 300 W, the RMS values decrease from 5.57 nm to 4.70 nm and average roughness values decrease from 4.35 nm to 3.63 nm. In case of (b), by increasing the input power from 250 W to 300 W, the RMS values decrease from 7.86 nm to 6.55 nm and average roughness values decrease from 5.98 nm to 5.13 nm. By comparing the samples without bias voltage and samples with a bias voltage, we observe that the samples without bias voltage have lower RMS. It can be seen (Fig. 5) that the thickness of the film decreases with a bias voltage. An increase in the substrate bias voltage causes an increase in the flux and energy of the ions bombardment of the substrate surface. The atoms etch the film, penetrate, will be trapped, and lead to film growth defects. Therefore, it increases the roughness of the films.

As the RF power increases from 250W to 300 W, the roughness of the film decreases. The ionization degree of target materials is small at lower RF power. The relative concentration of large-mass species is more than that of small-mass species. Meanwhile, at low RF power, the ion kinetic energy is low, the species reaching the substrate or the film surface are mainly larger-mass species. These larger-mass species are appropriate to form clusters and aggregates in the gas phase before deposition. Such clusters form preferentially on the surface. It leads to more defects such as the asperities on the film surface. The roughness values of the films deposited are given in Table 2.

Table 2: Roughness parameters of deposited TiCrN thin films.

Sample number	RMS (nm)	R_a (nm)
1	4.70	3.63
2	5.57	4.35
3	6.55	5.13
4	7.86	5.98

3.4 Contact angle results

We measured the contact angle of TiCrN thin films using the sessile drop method, before and after deposition. As seen in Fig. 10, before the deposition process, our Si substrate had a contact angle value of fewer than 90 degrees (~ 61.7^0) and it is a hydrophilic surface. After the deposition process, the contact angle of all samples increased. The interesting point is the relationship between the roughness and the contact angle values of the coatings. As the roughness of the surfaces increases, their contact angle increases, and vice versa. The results show that the contact angle of the samples with a bias voltage is more than the samples without any bias voltage. This means that by

giving the bias voltage to the substrate, the surface of the coating is being hydrophobic, whereas it has previously been hydrophilic. On the other hand, with increasing the input power in both sets of samples, the contact angle decreases. As can be seen the Fig. 10, sample 4 has the highest contact angle value and is more hydrophobic than the rest of the samples.

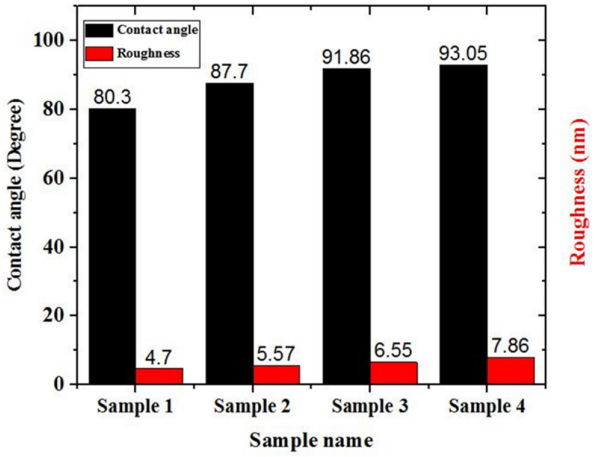

Figure 10. Variation of sample contact angle with different samples.

The water contact angle depends on the surface roughness, while can be explained by two models: Wenzel and Cassie-Baxter models [34]. Based on the Cassie-Baxter model, when the roughness of the surface increase, the proportion of air pocket increases correspondingly, and the contact angle should increase in the order of surface roughness from small to large. This is consistent with our results.

4 Conclusions

The ternary nitride TiCrN nanostructured coatings were deposited successfully on Si (100) substrate at room temperature using the RF magnetron sputtering method. The effects of the input RF power and bias voltage on the structure and properties of the TiCrN coatings has been studied. The results of the GIXRD analysis show that the TiCrN thin film peaks appeared in samples with substrate bias=-70 V. The intensity of TiCrN (220) diffraction peak decreases as the RF power increases from 250 W in sample 4 to 300 W in sample 3. When the bias voltage increased from 0 V to -70 V, two phases related to TiCrN were observed. The FESEM images demonstrate quite a uniform surface with the homogenous distribution of the grain sizes. The cross-sectional FESEM images show that the thickness of the film decreases with a bias voltage. With increasing the input RF power from 250 W to 300 W without bias voltage, deposition rate increases from 11 nm/min to 13 nm/min. As the RF power increases from 250W to 300 W, the roughness of the film decreases. The contact angle of the samples with bias voltage was more than the samples without voltage.

References

[1] A. K. Tareen, G. S. Priyanga, S. Behara, T. Thomas, M. Yang, "Mixed ternary transition metal nitrides: A comprehensive review of synthesis, electronic structure, and properties of engineering relevance. Progress in Solid State Chemistry, **53** (2019) 1-26.

[2] P. J. McGinn, "Thin-Film Processing Routes for Combinatorial Materials Investigations—A Review." ACS Combinatorial Science, **21** (2019) 501.

[3] N. Witit-Anun, A. Teekhaboot, "Effect of Ti Sputtering Current on Structure of TiCrN Thin Films Prepared by Reactive DC Magnetron Co-Sputtering." Key Engineering Materials, **675-676** (2016) 181.

[4] N. Bensalah, F.Z. Kamand, N. Mustafa, M. Matalqeh, "Silicon–Germanium bilayer sputtered onto a carbon nanotube sheet as anode material for lithium–ion batteries." Journal of Alloys and Compounds, **811** (2019) 152088.

[5] B. Navinšek, P. Panjan, A. Cvelbar, "Characterization of low temperature CrN and TiN (PVD) hard coatings." Surface and Coatings Technology, **74-75** (1995) 155.

[6] S. Kislitsin, I. Gorlachev, V. Uglov, "Effects of Irradiation with Low-Energy and High-Energy Krypton Ions on the Structure of TiCrN Coatings." Acta Physica Polonica A, **128** (2015) 818.

[7] S. Chen, D. Luo, G. Zhao, Investigation of the Properties of TixCr1-xN Coatings Prepared by Cathodic Arc Deposition, Physics Procedia, **50** (2013) 163.

[8] C. Mendibide, P. Steyer, J. Fontaine, P. Goudeau, "Improvement of the tribological behaviour of PVD nanostratified TiN/CrN coatings — An explanation." Surface and Coatings Technology, **201** (2006) 4119.

[9] T. Deeleard, S. Chaiyakun, A. Pokaipisit, P. Limsuwan, "Effects of Vanadium Content on Structure and Chemical State of TiVN Films Prepared by Reactive DC Magnetron Co-Sputtering." Materials Sciences and Applications, **4** (2013) 556.

[10] H. S. M. J. G. Han, H. M. Lee, L. R. Shaginyan, "Microstructure and mechanical properties of Ti–Ag–N and Ti–Cr–N superhard nanostructured coatings." Surface and Coatings Technology, **743** (2003) 174738

[11] H. S. Choi, D. H. Han, W. H. Hong, J. J. Lee, "(Titanium, chromium) nitride coatings for bipolar plate of polymer electrolyte membrane fuel cell." Journal of Power Sources, **189** (2009) 966.

[12] A. Buranawong, N. Witit-anun, S. Chaiyakun, A. Pokaipisit, P. Limsuwan, "The effect of titanium current on structure and hardness of aluminium titanium nitride deposited by reactive unbalanced magnetron co-sputtering." Thin Solid Films, **519** (2011) 4963.

[13] X. Z. Ding, A.L.K. Tan, X.T. Zeng, C. Wang, T. Yue, C.Q. Sun, "Corrosion resistance of CrAlN and TiAlN coatings deposited by lateral rotating cathode arc." Thin Solid Films, **516** (2008) 5716.

[14] A. Obrosov, R. Gulyaev, M. Ratzke, A. Volinsky, S. Bolz, M. Naveed, S. Weiß, "XPS and AFM Investigations of Ti-Al-N Coatings Fabricated Using DC Magnetron Sputtering at Various Nitrogen Flow Rates and Deposition Temperatures." Metals, **7** (2017) 52.

[15] A. Z. Ait-Djafer, N. Saoula, H. Aknouche, B. Guedouar, N. Madaoui, "Deposition and characterization of titanium aluminum nitride coatings prepared by RF magnetron sputtering." Applied Surface Science, **350** (2015) 6.

[16] S. Chinsakolthanakorn, A. Buranawong, S. Chiyakun, P. Limsuwan, Effects of Titanium Sputtering Current on Structure and Morphology of TiZrN Films Prepared by Reactive DC Magnetron Co-Sputtering, Materials Sciences and Applications, **4** (2013) 689.

[17] V. V. Uglov, D. P. Rusalski, S. V. Zlotski, A. V. Sevriuk, G. Abadias, S. B. Kislitsin, K. K. Kadyrzhanov, I. D. Gorlachev, S. N. Dub, "Stability of Ti–Zr–N coatings under Xe-ion irradiation." Surface and Coatings Technology, **204** (2010) 2095.

[18] J. Lin, B. Mishra, J. J. Moore, W. D. Sproul, J. A. Rees, "Effects of the substrate to chamber wall distance on the structure and properties of CrAlN films deposited by pulsed-closed field unbalanced magnetron sputtering (P-CFUBMS)." Surface and Coatings Technology, **201** (2007) 6960.

[19] X. S. Miao, Y. C. Chan, E. Y. B. Pun, "Protective AlCrN film for organic photoconductors." Thin Solid Films, **324** (1998) 180.

[20] X. Chen, Y. Xi, J. Meng, X. Pang, H. Yang, "Effects of substrate bias voltage on mechanical properties and tribological behaviors of RF sputtered multilayer TiN/CrAlN films." Journal of Alloys and Compounds, **665** (2016) 210.

[21] Q. M. Mehran, A. R. Bushroa, M. A. Fazal, M. M. Quazi, "Scratch adhesion characteristics of PVD Cr/CrAlN multilayer coating deposited on aerospace AL7075-T6 alloy." Pigment & Resin Technology, **44** (2015) 364.

[22] Q. M. Mehran, A. R. Bushroa, M. A. Fazal, "Evaluation of CrAlN multilayered coatings deposited by PVD magnetron sputtering." Journal of Adhesion Science and Technology, **29** (2015) 2076.

[23] C. Zhuang, Z. Li, S. Lin, "Effect of annealing process on atomic-scale structure, dislocation and mechanical behaviour of nano-grained Al–Cr–N thin films." Surface Engineering, **33** (2016) 204.

[24] Y. Lv, L. Ji, X. Liu, H. Li, H. Zhou, J. Chen, "The structure and properties of CrAlN films deposited by mid-frequency unbalanced magnetron sputtering at different substrate bias duty cycles." Surface and Coatings Technology, **206** (2012) 3961.

[25] X. Wang, L. S. Wang, Z. B. Qi, G. H. Yue, Y. Z. Chen, Z. C. Wang, D. L. Peng, "Investigation on the structure and properties of AlxCr1−xN coatings deposited by reactive magnetron co-sputtering." Journal of Alloys and Compounds, **502** (2010) 243.

[26] M. Fellah, L. Aissani, M. A. Samad, S. Mechacheti, M. Z. Touhami, A. Montagne, A. Iost, "Characterisation of R.F. magnetron sputtered Cr-N, Cr-Zr-N and Zr-N coatings." Transactions of the IMF, **95** (2017) 261.

[27] S. Khamseh, H. Araghi, "A study of the oxidation behavior of CrN and CrZrN ceramic thin films prepared in a magnetron sputtering system." Ceramics International, **42** (2016) 9988.

[28] S. M. Aouadi, K. C. Wong, K. A. R. Mitchell, F. Namavar, E. Tobin, D. M. Mihut, S. L. Rohde, "Characterization of titanium chromium nitride nanocomposite protective coatings." Applied Surface Science, **229** (2004) 387.

[29] G. A. Zhang, P. X. Yan, P. Wang, Y. M. Chen, J. Y. Zhang, "The structure and tribological behaviors of CrN and Cr–Ti–N coatings." Applied Surface Science, **253** (2007) 7353.

[30] C. H. Hsu, C. K. Lin, K. H. Huang, K. L. Ou, "Improvement on hardness and corrosion resistance of ferritic stainless steel via PVD-(Ti,Cr)N coatings." Surface and Coatings Technology, **231** (2013) 380.

[31] M. Huang, Z. Chen, M. Wang, Y. Li, Y. Wang, "Microstructure and properties of TiCrN coatings by arc ion plating." Surface Engineering, **32** (2016) 284.

[32] Q. Wang, F. Zhou, J. Yan, "Evaluating mechanical properties and crack resistance of CrN, CrTiN, CrAlN and CrTiAlN coatings by nanoindentation and scratch tests." Surface and Coatings Technology, **285** (2016) 203.

[33] S. Y. Lee, G. S. Kim, J. H. Hahn, "Effect of the Cr content on the mechanical properties of nanostructured TiN/CrN coatings." Surface and Coatings Technology, **177-178** (2004) 426.

[34] W. M. Sigmund, S. H. Hsu, Cassie–Baxter Model, in: E. Drioli, L. Giorno (Eds.) Encyclopedia of Membranes, Springer Berlin Heidelberg, Berlin, Heidelberg (2016) 310-311.